AFRL-RY-WP-TP-2013-0163

LOW FREQUENCY PLASMA TURBULENCE AS A SOURCE OF CLUTTER IN SURVEILLANCE AND COMMUNICATION (POSTPRINT)

V. Sotnikov and T. Kim

Antennas & Electromagnetics Technology Branch
Multispectral Sensing & Detection Division

E. Mishin

Air Force Research Laboratory
Kirtland, AFB

W. Amatucci, G. Ganguli, E. Tejero, and T.A. Mehlhorn

Naval Research Laboratory

I. Paraschiv

University of Nevada at Reno

AUGUST 2013
Interim

AIR FORCE RESEARCH LABORATORY
SENSORS DIRECTORATE
WRIGHT-PATTERSON AIR FORCE BASE, OH 45433-7320
AIR FORCE MATERIEL COMMAND
UNITED STATES AIR FORCE

REPORT DOCUMENTATION PAGE

Form Approved
OMB No. 0704-0188

1. REPORT DATE *(DD-MM-YY)*	2. REPORT TYPE	3. DATES COVERED *(From - To)*
August 2013	Technical Paper Posprint	1 October 2011 – 30 September 2012

4. TITLE AND SUBTITLE
LOW FREQUENCY PLASMA TURBULENCE AS A SOURCE OF CLUTTER IN SURVEILLANCE AND COMMUNICATION (POSTPRINT)

5a. CONTRACT NUMBER
In-house

5b. GRANT NUMBER

5c. PROGRAM ELEMENT NUMBER
61102F

6. AUTHOR(S)
V. Sotnikov and T. Kim (AFRL/RYMH)
E. Mishin (AFRL/RV)
W. Amatucci, G. Ganguli, E. Tejero, and T.A. Mehlhorn (Naval Research Laboratory)
I. Paraschiv (University of Nevada at Reno)

5d. PROJECT NUMBER
3001

5e. TASK NUMBER
12

5f. WORK UNIT NUMBER
Y0R7

7. PERFORMING ORGANIZATION NAME(S) AND ADDRESS(ES)
Antennas & Electromagnetics Technology Branch
Multispectral Sensing & Detection Division
Air Force Research Laboratory, Sensors Directorate
Wright-Patterson Air Force Base, OH 45433-7320
Air Force Materiel Command, United States Air Force

Kirtland AFB
Naval Research Laboratory
University of Nevade at Reno

8. PERFORMING ORGANIZATION REPORT NUMBER
AFRL-RY-WP-TP-2013-0163

9. SPONSORING/MONITORING AGENCY NAME(S) AND ADDRESS(ES)
Air Force Research Laboratory , Sensors Directorate
Wright-Patterson Air Force Base, OH 45433-7320
Air Force Materiel Command
United States Air Force

Air Force Office of Scientific Research Public Affairs (AFOSR)
875 North Randolph Street
Arlington, VA 22203-1768

10. SPONSORING/MONITORING AGENCY ACRONYM(S)
AFRL/RYMH

11. SPONSORING/MONITORING AGENCY REPORT NUMBER(S)
AFRL-RY-WP-TP-2013-0163

12. DISTRIBUTION/AVAILABILITY STATEMENT
Approved for public release; distribution unlimited.

13. SUPPLEMENTARY NOTES
Journal article published in Proceeding of the AMOS Conference, Sept 2012. ©2012 AMOS. The U.S. Government is joint author of the work and has the right to use, modify, reproduce, release, perform, display or disclose the work.PAO Case Number 88ABW-2012-5182, Clearance Date 28 September 2012. Report contains color.

14. ABSTRACT
Presence of plasma turbulence can strongly influence propagation properties of electromagnetic signals used for surveillance and communication. In particular, we are interested in the generation of low frequency plasma turbulence in the form of coherent vortex structures coexisting with short scale density irregularities and of lower hybrid turbulence. Lower-hybrid type density irregularities are excited by plasma flows with velocity shear, whereas interchange or flute type oscillations in magnetized plasma are associated with Rayleigh-Taylor type instability. These types of density irregularities play important role in refraction and scattering of high frequency electromagnetic signals propagating in the earth ionosphere, inside a plasma sheath of reentry and hypersonic vehicles and in many other applications. We will discuss generation of low frequency density irregularities due to the presence of plasma flows with velocity shear and interchange instability.

15. SUBJECT TERMS
plasma turbulence, electromagnetic signals

16. SECURITY CLASSIFICATION OF:			17. LIMITATION OF ABSTRACT:	18. NUMBER OF PAGES	19a. NAME OF RESPONSIBLE PERSON (Monitor)
a. REPORT	b. ABSTRACT	c. THIS PAGE			Vladimir Sotnikov
Unclassified	Unclassified	Unclassified	SAR	24	19b. TELEPHONE NUMBER *(Include Area Code)* N/A

Low Frequency Plasma Turbulence as a Source of Clutter in Surveillance and Communication

V. Sotnikov, T. Kim
Air Force Research Laboratory (AFRL/RY), Wright Patterson AFB, OH 45433

E. Mishin
Air Force Research Laboratory (AFRL/RV), Kirtland AFB, NM 87117

W. Amatucci, G. Ganguli, E. Tejero and T.A. Mehlhorn
Naval Research Laboratory (NRL/PPD), Washington, DC 20375

I. Paraschiv
University of Nevada at Reno, NV 89523

Abstract

Presence of plasma turbulence can strongly influence propagation properties of electromagnetic signals used for surveillance and communication. In particular, we are interested in the generation of low frequency plasma turbulence in the form of coherent vortex structures coexisting with short scale density irregularities and of lower hybrid turbulence. Lower-hybrid type density irregularities are excited by plasma flows with velocity shear, whereas interchange or flute type oscillations in magnetized plasma are associated with Rayleigh-Taylor type instability. These types of density irregularities play important role in refraction and scattering of high frequency electromagnetic signals propagating in the earth ionosphere, inside a plasma sheath of reentry and hypersonic vehicles and in many other applications. We will discuss generation of low frequency density irregularities due to the presence of plasma flows with velocity shear and interchange instability.

1. Introduction

The scattering of high-frequency (HF) electromagnetic (EM) waves is a fundamental phenomenon in plasma physics. In a stable plasma EM scattering occurs due to the thermal electron density fluctuations and it is known as “Thomson scattering” [1]. Due to nonlinear interaction of waves in plasma, scattering can also arise from single waves excited in the plasma and is explained as three-wave nonlinear interaction [2]. Scattering can also take place due to interaction of HF waves with electrostatic solitons [3] or from charged dust particles [4]. In the present paper we will analyze formation of plasma density irregularities due to development of lower hybrid and interchange instabilities. These types of density irregularities play an important role in analysis of high frequency EM scattering and refraction in the ionospheric plasma. The reason for this is that the spatial scales of these plasma waves are comparable or smaller than typical wavelengths of EM signals used for surveillance, communication and OTH radar applications.

In the terrestrial high-latitude (auroral) magnetosphere and ionosphere, whistler-lower-hybrid fluctuations in their electromagnetic or electrostatic limits are usually found in association with energetic electron beams along the geomagnetic field and/or anisotropic electron distributions. In particular, the energetic electron acceleration within the terrestrial auroral region results in the emission of short-wavelength, primarily electrostatic waves near the resonance cone of the whistler-lower-hybrid branch [5]. Another source of enhanced lower hybrid waves in the auroral ionosphere is related to strongly sheared plasma flows driven by structured electric fields in the vicinity of small scale auroral arcs [6].

At subauroral latitudes, lower hybrid/fast magnetosonic waves accompany such well-known space weather phenomena as subauroral ion drifts (SAID) and subauroral polarization streams (SAPS) [7,8] . Figure 1.1 presents overview of one of such events occurred on 18 March 2002 when three independent spacecraft (Cluster, DMSP, and Polar) crossed the SAID channel virtually at the same time and within the same magnetic tube. It is seen that the wave activity is abruptly enhanced inside the SAID channel, just interior to the plasmaspere's boundary (the plasmapause).

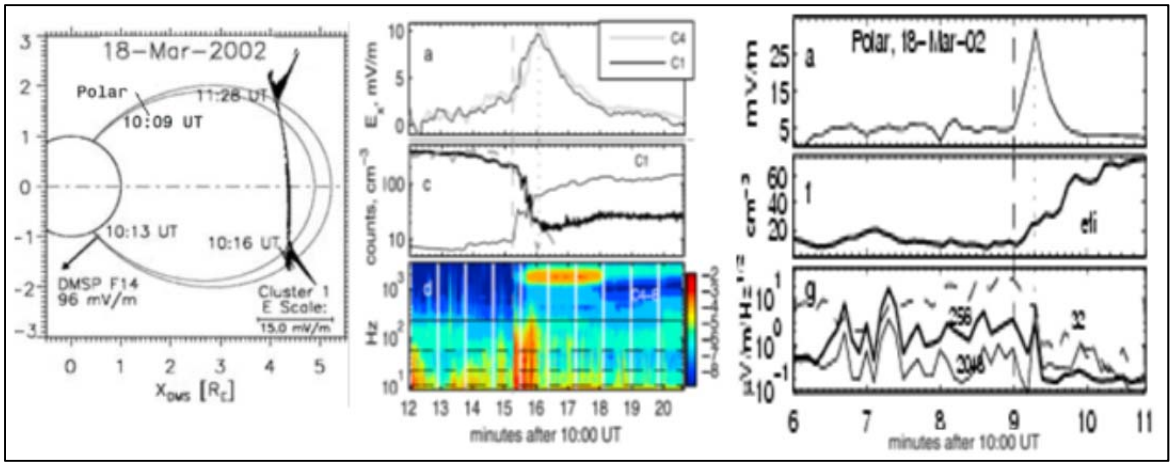

Figure 1.1 (left panel) World-line plots of the Cluster, DMSP, Polar satellites during the 18-March-2002 substorm event. The SAID channels from Cluster 1 (C1) are superimposed. Shown in the middle are (top) the C1/C4 outward electric field E_x in the inertial frame, (mid) C1/EDI 1-keV electron counts (thick line) and the cold plasma density n_0 (thin), and (bottom) C4/STAFF frequency-time spectrograms for the electric spectral power in $(mV/m)^2/Hz$ (in log scale). Horizontal lines indicate the lower hybrid resonance (solid) and the 10th, 4th, and 2nd harmonics of the H^+-ion gyrofrequency (dashed), derived from the observed magnetic field. Shown on the right are the features of the northern SAID channel from Polar: (top) the outward electric field, (mid) the plasma density, and (bottom) spectral amplitudes of electric fields at 32 (dashed line), 256 (thick), and 2048 (thin) Hz.

The remainder of this paper is organized as follows: In Section 2, excitation of the lower hybrid instability by flows with velocity shear in the presence of electron-neutral collisions is analyzed. Linearized equations for the lower hybrid eigenmodes inside a plasma slab with velocity shear will be derived and solved numerically. Numerical solution is based on the implementation of the shooting code. In Section 3, nonlinear equations describing interaction of the lower hybrid waves inside a plasma flow with velocity shear with the low frequency ion acoustic oscillations will be derived, and dispersion equation for the modified decay instability will be presented. In Section 4, the results of the laboratory experiments in the NRL Space Chamber on excitation of lower hybrid turbulence by **ExB** flows with velocity shear will be presented. In Section 5, linear and nonlinear stages of interchange instability with the ionospheric plasma parameters corresponding to the equatorial F-layer will be discussed. In the description of the interchange instability we retain finite ion Larmor radius effects. Inclusion of spatial scales comparable with the ion Larmor radius is important for the analysis of radar generated high-frequency EM waves interacting with density irregularities associated with the equatorial spread F in the ionosphere. A brief summary and applications are contained in Section 6.

2. Excitation of Lower Hybrid waves by a flow with velocity shear

In this Section we will analyze instability of a plasma flow with a transverse velocity shear scale length much smaller than the ion gyroradius but larger than the electron gyroradius. As shown in [9,10], under these conditions electrostatic oscillations with the frequencies above the lower hybrid frequency

$$\omega_{LH}^2 = \frac{\omega_{pi}^2}{1 + \frac{\omega_{pe}^2}{\omega_{ce}^2}} \tag{2.1}$$

can be excited. In (2.1) ω_{pe} and ω_{pi} are the corresponding electron and ion plasma frequencies and ω_{ce} is the electron cyclotron frequency. Below in the hydrodynamic approximation we will derive the equation for excitation of oscillations in the frequency range just above the lower hybrid frequency ω_{LH}. In this equation we will include wave dispersion due to the thermal effects, electron neutral collision frequency and nearly perpendicular to the magnetic field propagation wave vectors with $\frac{k_z^2}{k_y^2} << \frac{m}{M}$ (m and M are electron and ion masses respectively), k_y - is the wave vector perpendicular to an external magnetic field and k_z – is the wave vector of oscillations along the magnetic field. Electrons in the lower hybrid oscillations are magnetized, but ions are unmagnetized. The external electric filed varies along the x-direction $E_{0x}(x)$ and creates electron flow with velocity shear directed along the y-direction $V_{0y}(x)$ (see Figure 2.1). The width of the layer with electric field inhomogeneity is smaller than the ion Larmor radius. In such a system, we have electron flow with velocity shear moving in y-direction, whereas ions, being unmagnetized, do not experience **ExB** drift and are at rest in the laboratory coordinate system. We will use linearized electron momentum equation in the drift approximation which also contains electron neutral collisions term and linearized ion momentum equation for

unmagnetized ions. Using also continuity equations for electrons and ions and Poisson equation for the electrostatic potential of a lower hybrid wave, we can arrive to the following linearized equation which describes wave excitation in the non-local approximation:

$$\frac{\partial^2}{\partial t^2}[(\frac{\omega_{pi}^2}{\omega_\alpha^2}(1+R^2\Delta)\hat{L}_z^2\Delta\Phi+\omega_{pe}^2\frac{\partial^2\Phi}{\partial z^2}+\nu_{en}((1+2\frac{\omega_{pe}^2}{\omega_{ce}^2})\hat{L}_z+\frac{\omega_{pe}^2}{\omega_{ce}^2})\Delta\Phi-$$

$$\frac{\omega_{pe}^2}{\omega_{ce}^2}(\hat{L}_z+\nu_{en})\frac{\partial^2 V_{0y}}{\partial x^2}\frac{\partial\Phi}{\partial y}]+\omega_{pi}^2[\hat{L}_z^2+\nu_{en}\hat{L}_z]\Delta\Phi=0 \qquad (2.2)$$

In equation (1) ν_{en} is an electron-neutral collision frequency, $V_{0y}(x)$ is the flow velocity and operator $\hat{L}_z$ is defined as: $\hat{L}_z=\frac{\partial}{\partial t}+V_{0y}(x)\frac{\partial}{\partial y}$.

We are interested in the solution of the equation (1) which represent waves propagating along the y and z directions inside a plasma slab and the solution in the form of the eigenfunction in the x-direction of the flow inhomogeneity:

$$\Phi\sim\Psi(x)\exp(-i\omega t+k_y y+k_z z) \qquad (2.3)$$

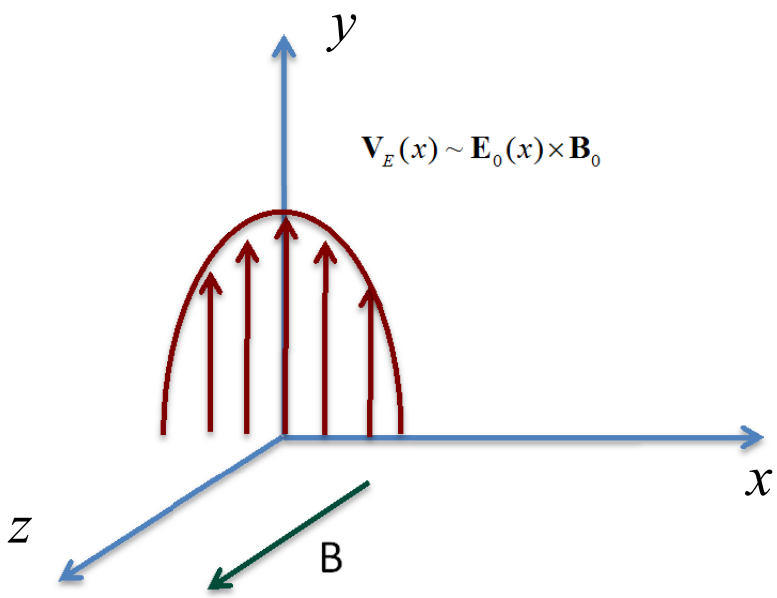

Figure 2.1. In this figure a nonuniform electric field $E_{0x}(x)$ and an external magnetic field B_{0z} create a nonuniform electron flow with velocity shear along the *y*-direction.

We set $x = 0$ at the conducting surface of the vehicle and require

$$\phi\left(x = 0\right) = 0. \tag{2.4}$$

In the free space beyond the sheath edge at $x = L$, the potential $\phi\left(x\right) = \phi\left(L\right)\exp\left[-k\left(x - L\right)\right]$ so that

$$\left[\frac{d\phi}{dx} + k\phi\right]_{x=L} = 0. \tag{2.5}$$

Equations (2.2) ,(2.4) and (2.5) constitute the eigenvalue problem to be solved numerically for the complex eigenfrequency ω using a standard shooting method [11].
Using equation (2.2) for conditions used in Ganguli *et al.* and neglecting thermal dispersion of lower hybrid waves (R = 0), electron-neutral collisions ($\nu_{en} = 0$) and restricting analysis to the waves with $k_z = 0$, the shooting code recovers the previously published solutions $\omega = (1.89 + i1.94)\omega_{LH}$ [9]From this point using equation (2.2), the shooting code was used to investigate the effect of finite electron-neutral collisions on the mode. Figure 2.2 shows the real frequency (solid black line) and growth rate (dashed red line) normalized to the lower hybrid frequency as function of electron-neutral collision frequency normalized to the electron cyclotron frequency for plasma conditions similar to those from published experimental observations of this instability [12]: $\omega_{pe}/\Omega_e = 8.0$, $v_E/\Omega_e L_E = 13.6$, $k_y L_E = 0.5$, $k_z L_E = 0$, and argon ions. The following electric field profile was used in the code:

$$E_{0x}(x) = E_0 \sec h^2(\frac{x}{L_E}) \tag{2.6}$$

where L_E is the velocity shear scale length in the electron flow and the shear flow velocity along the y-direction is defined as:

$$\mathrm{V}_{0y}(x)\mathbf{e}_y = c\frac{\mathbf{E}_0(x)\times\mathbf{B}_0}{B_0^2} \tag{2.7}$$

where c – is the speed of light.
Results of numerical solution of equation (2.2) with inclusion of electron-neutral collisions, but with omission of thermal dispersion and with $k_z = 0$ are presented by Figure 2.2. It can be seen that presence of weak collisions has a strong effect on both the growth rate and real frequency, though the mode is not completely stabilized. We stop at $\nu_{en} \sim 0.1\omega_{ce}$ to remain in the regime where the drift approximation is valid. However, it is expected that $\upsilon_{en} \sim \Omega_e$ is needed before collisions could totally suppress excitation of the mode.

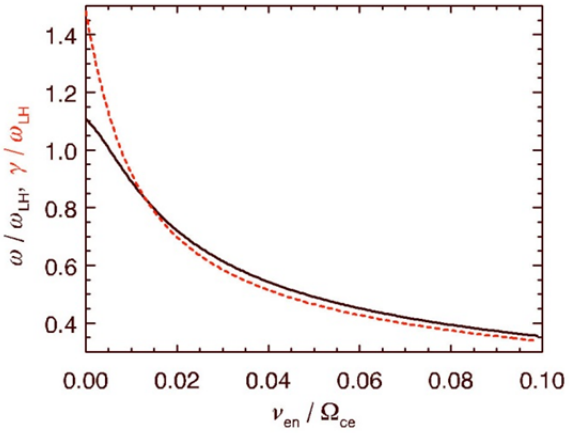

Figure 2.2: Normalized real frequency (solid black line) and growth rate (dashed red line) dependence on normalized collision frequency.

To obtain solution for the frequency and the growth rate of excited modes in the local approximation, we again will use equation (2.2) neglecting thermal dispersion of lower hybrid waves(R=0), electron-neutral collisions ($\nu_{en} = 0$) and restricting analysis to the waves with $k_z = 0$. This will allow us to examine the qualitative behavior of this instability without employing the full numerical solution. To arrive at the local approximation for the lower hybrid modes, we start from:

$$\frac{\mathrm{d}^2\phi}{\mathrm{d}\overline{x}^2} - \overline{\kappa}^2\phi = 0,$$

where

$$\overline{\kappa}^2 = \overline{k}_y^2 - \frac{\delta^2}{\delta^2+1}\frac{\overline{\omega}^2}{\overline{\omega}^2-1}\frac{\overline{k}_y\bar{v}_E''}{\bar{\omega}-\overline{k}_y\bar{v}_E},$$

and $\delta = \omega_{pe}/\Omega_e$, $\bar{k}_y = k_y L_E$, $\overline{\omega} = \omega/\omega_{LH}$, and $\overline{v}_E = v_E/\omega_{LH}\,L_E$. We obtain the local dispersion relation by taking $\overline{\kappa}^2 = 0$ and using the values for $\overline{v}_E$ and $\overline{v}_E''$ at $x = 0$ as in Romero *et al.* [9]. This results in a cubic equation for ω:

$$\overline{\omega}^3 + \overline{k}_y\overline{v}_{E0}\left(\frac{2}{\overline{k}_y^2}\frac{\delta^2}{\delta^2-1} - 1\right)\overline{\omega}^2 - \overline{\omega} + \overline{k}_y\overline{v}_{E0} = 0,$$

Figure 1.3 shows the local and non-local solutions for the following parameters: $\delta = 8.0$, $\overline{v}_E = 1.1$, $k_y L_E = 0.5$, $k_z L_E = 0$, and argon ions. The local solution does a good job of approximating the general behavior of the non-local solutions, but more importantly, it represents a good operating regime for studying the non-linear behavior of this mode. The maximum growth rate occurs for a real frequency just above the lower hybrid frequency, and the mode only exists for a small band of perpendicular wave numbers.

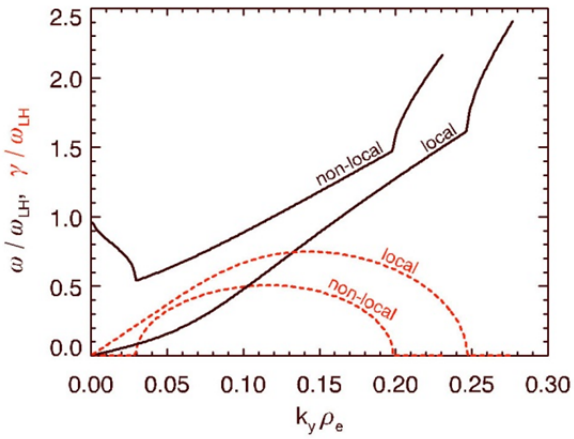

Figure 1.3: Normalized real frequency (solid black line) and growth rate (dashed red line) dependence on normalized perpendicular wave number comparing local and non-local solutions.

3. Nonlinear interaction of lower hybrid and ion acoustic waves

It is well known that the most effective mechanism for saturation of the lower hybrid instability is connected with the decay and modified decay instabilities which occur due to interaction of the excited lower hybrid waves with the ion acoustic oscillations [13, 14]. In the experiments described in Section 4, the electron temperature was much larger than the ion temperature with $\frac{T_e}{T_i} \sim 10$. This justifies implementation of the nonlinear scheme with involvement of ion acoustic waves instead of the nonlinear interaction scheme based on induced scattering on electrons. System of equations for the electrostatic potential of lower hybrid waves excited in a system consisting of unmagnetized ions and moving through them in y-direction magnetized electrons with velocity shear in x-direction with the speed $V_{0y}(x)$ and nonlinearly coupled with ion acoustic oscillations is presented below. Density perturbations in ion acoustic oscillations are defined as δn. This system of equations has the following form:

$$\frac{\partial^2}{\partial t^2}[(\frac{\omega_{pi}^2}{\omega_\alpha^2}(1+R^2\Delta)\hat{L}_z^2\Delta\Phi+\omega_{pe}^2\frac{\partial^2\Phi}{\partial z^2}-\frac{\omega_{pe}^2}{\omega_{ce}^2}\hat{L}_z\frac{\partial^2 V_{0y}}{\partial x^2}\frac{\partial\Phi}{\partial y}]+\omega_{pi}^2\hat{L}_z^2\Delta\Phi=\frac{\omega_{pe}^2}{\omega_{ce}^2}\frac{\partial^2}{\partial t^2}\hat{L}_z\{\frac{\delta n}{n_0},\Phi\} \quad (3.1)$$

$$\frac{\partial^2\delta n}{\partial t^2}-(V_{Ti}^2+V_s^2)\Delta\delta n=-\frac{i}{4\pi M}\frac{\omega_{pe}^2}{\omega_{ce}\omega_\alpha}\Delta\{\Phi,\Phi^*\} \quad (3.2)$$

In equations (3.1) and (3.2) Poisson brackets $\{a,b\}$ are defined as $\{a,b\}=\frac{\partial a}{\partial x}\frac{\partial b}{\partial y}-\frac{\partial a}{\partial y}\frac{\partial b}{\partial x}$ and $\hat{L}_z=\frac{\partial}{\partial t}+V_{0y}(x)\frac{\partial}{\partial y}$.

Below, in the local approximation we will derive dispersion equation for modified decay of excited lower hybrid waves and find the estimate for the threshold of this instability. In the

absence of the electron flow, modified decay of magnetosonic waves in the vicinity of the lower hybrid frequency was analyzed in [15].

We will examine the case when the pump wave is excited due to the presence of velocity shear in the electron flow. The parametric decay of a pump wave into two satellites in vicinity of the lower hybrid frequency and low-frequency ion acoustic type mode represented by the low-frequency density fluctuations can be describe as follows. We will introduce the pump lower hybrid wave:

$$\Phi_{\mathbf{k}_0} = (\frac{1}{2}\varphi_{\mathbf{k}_0} e^{i\alpha_{\mathbf{k}_0}}) e^{i(\mathbf{k}_0\mathbf{r}-\omega_{\mathbf{k}_0}t)} + c.c = \Psi_{\mathbf{k}_0} e^{i(\mathbf{k}_0\mathbf{r}-\omega_{\mathbf{k}_0}t)} + c.c \tag{3.3}$$

As well as Anti-Stokes:

$$\Phi_{\mathbf{k}_1} = (\frac{1}{2}\varphi_{\mathbf{k}_1} e^{i\alpha_{\mathbf{k}_1}}) e^{i(\mathbf{k}_1\mathbf{r}-\omega_{\mathbf{k}_1}t)} + c.c = \Psi_{\mathbf{k}_1} e^{i(\mathbf{k}_1\mathbf{r}-\omega_{\mathbf{k}_1}t)} + c.c \tag{3.4}$$

and Stokes satellites:

$$\Phi_{\mathbf{k}_2} = (\frac{1}{2}\varphi_{\mathbf{k}_2} e^{i\alpha_{\mathbf{k}_2}}) e^{i(\mathbf{k}_2\mathbf{r}-\omega_{\mathbf{k}_2}t)} + c.c = \Psi_{\mathbf{k}_2} e^{i(\mathbf{k}_2\mathbf{r}-\omega_{\mathbf{k}_2}t)} + c.c \tag{3.5}$$

For the ion acoustic type density fluctuations we will use:

$$\delta n_{\mathbf{k}_s} = (\frac{1}{2}\delta n_{\mathbf{k}_s} e^{i\alpha_{\mathbf{k}_s}}) e^{i(\mathbf{k}_s\mathbf{r}+\nu_{\mathbf{k}_s}t)} + c.c = \delta N_{\mathbf{k}_s} e^{i(\mathbf{k}_s\mathbf{r}+\nu_{\mathbf{k}_s}t)} + c.c \tag{3.6}$$

The following conditions on the wave vectors of two satellites $\mathbf{k}_1$ and $\mathbf{k}_2$ as well as the wave vector in ion acoustic perturbations $\mathbf{k}_s$ are imposed: $\mathbf{k}_1 = \mathbf{k}_0 + \mathbf{k}_s$ and $\mathbf{k}_2 = \mathbf{k}_0 - \mathbf{k}_s$. Now, using equations (3.1) and (3.2) the following dispersion equation for the modified decay instability of the lower hybrid waves interacting with low frequency ion acoustic density fluctuations can be derived:

$$\nu^2 = [(V_{Ti}^2 + V_s^2)k_s^2] - \frac{1}{4\pi M n_0}\frac{\omega_{pe}^2}{\omega_{ce}\omega_\alpha} k_s^2 [\mathbf{k}_0 \times \mathbf{k}_s]_z^2 \frac{\omega_{pe}^2}{\omega_{ce}} \omega_\alpha^2 \mid \Psi_{\mathbf{k}_0} \mid^2 \times$$

$$\times \{\frac{1}{D_{R\mathbf{k}_2}^*}\frac{[(\delta\omega_{\mathbf{k}_0} + k_{sy}V_{0m} + \nu)]}{[(\omega_{\mathbf{k}_0} - \omega_{\mathbf{k}2}) + \nu]} + \frac{1}{D_{R\mathbf{k}_1}}\frac{(\delta\omega_{\mathbf{k}_0} - k_{sy}V_{0m} - \nu)}{[(\omega_{\mathbf{k}_0} - \omega_{\mathbf{k}1}) - \nu]}\} \tag{3.7}$$

To obtain (3.7), we also used:

$$\omega_{\mathbf{k}} = \omega_{LH} + \delta\omega_{\mathbf{k}}; \quad \omega_{LH} \sim k_{0y}V_{0m}; \quad \frac{d^2V_{0y}}{dx^2} = -\frac{2V_{0m}}{L_E^2}$$

Finally, from equation (3.7) the following estimate for the threshold of the modified decay instability of the lower hybrid waves can be obtained:

$$\frac{E_0^2}{4\pi n_0 T_e} \geq \frac{m}{M}\frac{\omega_{ce}^2}{\omega_{pe}^2} \tag{3.8}$$

Using (3.8) it is also possible to estimate the amplitude of the low frequency ion acoustic type density fluctuations which appear in the system.

4. Experiments on excitation of lower hybrid turbulence in the NRL Space Chamber

In a series of experiments, Amatucci *et al.* [12] demonstrated that strongly sheared electron flows perpendicular to the background magnetic field with scale size smaller than an ion gyroradius but larger than an electron gyroradius can drive electrostatic oscillations near the lower hybrid frequency. These observations were consistent with the theoretical predictions of Ganguli et al. [8] and Ganguli and Romero [9] and lent s upport to the relaxation scenario for highly stressed magnetospheric boundary layers. For example, during intense solar activity, the plasma sheet boundary layer can become highly compressed, with gradients in the plasma across the layer self-consistently generating localized electric fields and highly sheared flows across the magnetic field. These sheared flows generate plasma instabilities that work to dissipate differential flows and widen the boundary layer. An analogous situation can arise in the flowing plasma surrounding a hypersonic vehicle, resulting in the generation of strong plasma turbulence.

The experiments on the generation of shear-driven lower hybrid waves were conducted in the Space Physics Simulation Chamber (SPSC) at the Naval Research Laboratory. The main chamber part of the SPSC consists of a 1.8 m diameter, 5 m long cylindrical vacuum vessel designed for controlled, scaled experiments of space plasma processes. For these experiments, a large area (~ 75 cm diameter) hot filament plasma source was placed at one end of the chamber, while a smaller filament source (~ 2 cm diameter) is placed at the opposite end. As can be seen in a schematic of the experimental setup in Figure 4.2, an isolated electrode blocks a small portion of the plasma generated by the large area source, which is filled with the plasma generated by the small plasma source. The blocking disk and the outer grid of the small source allow for control over the plasma potential of the small area plasma column. Strong radial dc electric fields can be generated by this steep variation of plasma potential across the cylindrical boundary layer between the two plasmas. This in conjunction with the filament heater currents on both sources enables independent control over the electric field and density gradients across the boundary of the two interpenetrating plasmas, simulating the stressed plasma sheet boundary layer conditions.

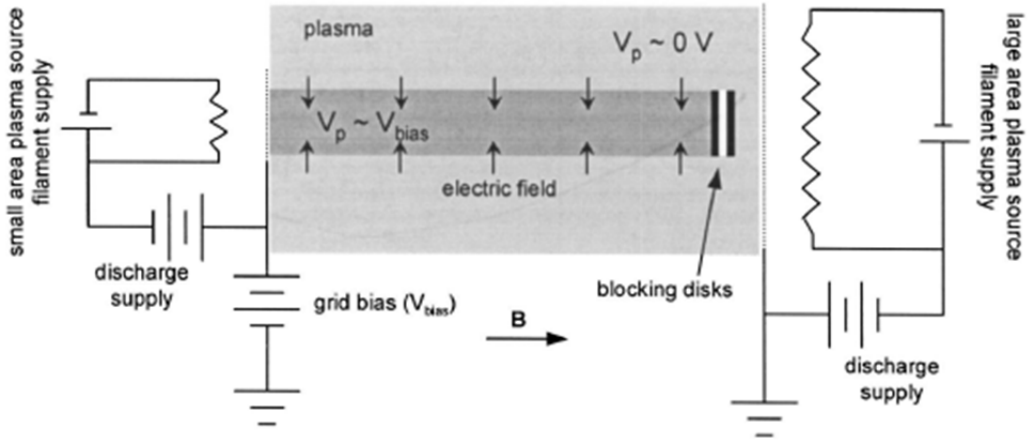

Figure 4.2: Schematic diagram of the experimental setup showing the two interpenetrating plasmas.

Typical parameters for the steady-state argon plasma are: plasma density n ~10^9-10^{10} cm^{-3}, ion and electron temperatures T_i ~0.05 eV and T_e ~0.25 eV, ion and electron thermal speeds v_{ti} ~ 5×10^4 cm/s and v_{te} ~ 2×10^7 cm/s, and an axial magnetic field B = 40 G. This yields ion and electron gyrofrequencies Ω_i ~1.5 kHz and Ω_e ~110 Mhz, ion and electron gyroradii ρ_i ~3.5 cm and ρ_e ~0.03 cm, and lower hybrid frequency f_{LH} ~400 kHz. The neutral density n_n is variable from 10^{11}-10^{14} cm^{-3}, and the plasma column diameter and effective length are 75 cm and 3 m, respectively.

Plasma potential was measured using radial emissive probes. The derivative of the resulting profile is the electric field profile. The measured electric field yields a typical transverse electric field scale length L_E from 0.6-1.0 cm (0.17-0.3 ρ_i) and the magnitude can be controlled up to 40 V/cm. Typical plasma potential (solid line without symbols) and electric field (dashed line) radial profiles can be seen in Figure 4.3. Since the electric field scale length is in the range $\rho_e < L_E < \rho_i$, the electrons **E**×**B** drift but the ions do not. For sufficiently strong electric fields, an instability with frequency in the lower hybrid frequency range is observed within the shear layer. Figure 4.3 shows an overlay of mode amplitude (solid circles) as a function of radial position localized to the edge of the transverse electron flow layer. A sample wave spectrum is also inset showing a mode with frequency ~780 kHz (~1.9f_{LH}), indicating that sheared transverse electron flows without the presence of a density gradient can drive lower hybrid waves.

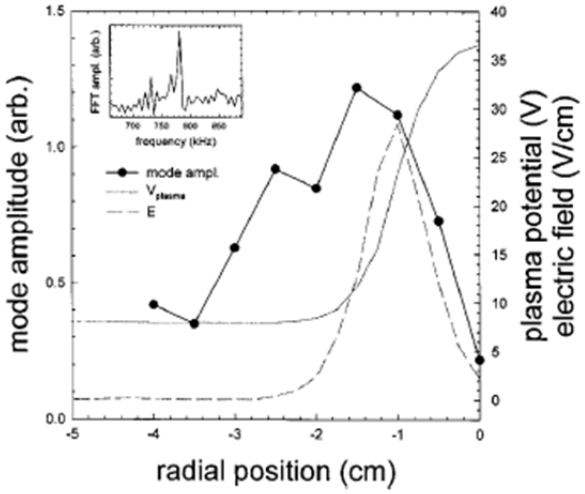

Figure 4.3: Radial profile of lower hybrid wave amplitude for the uniform density case and wave spectrum as inset.

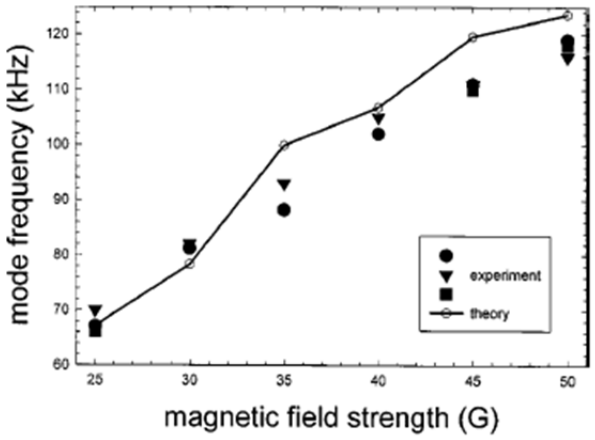

Figure 4.4: Comparison of experimentally observed (filled symbols) and theoretically predicted (line) values of mode frequency as a function of magnetic field strength.

Figure 4.4 shows a comparison between theoretically predicted mode frequency for these velocity shear-driven waves and the experimentally measure values as a function of the magnetic field strength. There is good agreement between the theoretical predictions and the measure mode frequencies. The observed instability also exhibits a threshold electric field (~7.5 V/cm) for the waves to appear. This coupled with the spatial localization of the mode amplitude to the shear layer suggests that the shear in the electron **E×B** flow is responsible for driving the observed lower hybrid waves.

While these experiments were scaled to magnetospheric boundary layer conditions, they could equally be applied to hypersonic vehicle plasmas. Future experimentation will focus on increasing the overall size of the flowing plasma region while maintaining the steep gradients. By driving the mode well in the nonlinearly saturate state, we will investigate the formation of turbulent plasma density structures and the effect of such structures on the scattering and transmission of electromagnetic waves.

5. Interchange instability in the ionospheric F-layer

Below we will present analysis of generation of density vorticies on the nonlinear stage of interchange instability[16 – 18]. Such density vorticies can play significant role in scattering of high-frequency EM waves generated on the nonlinear stage of excited instability. Such vorticies appear in the ionospheric F-layer and are part of the ionospheric clutter [19 – 22]. They also can exist in a plasma flow around a hypersonic vehicle and adversely effect sensors performance. This study is also relevant to a laser probing in a high energy density plasmas and for diagnostics of the edge plasma in tokamaks. Our analysis will be applicable to both low-beta and high-beta plasmas and will include finite ion Larmor radius effects [16, 17]. Inclusion of spatial scales comparable with the ion Larmor radius is important for the analysis of radar generated high-frequency EM waves interacting with density irregularities associated with the equatorial spread F in the ionosphere.

5.1 Basic Equations

Two-fluid macroscopic equations will be used to describe low-frequency interchange modes ($\omega << \Omega_i$, where ω is the frequency of the flute mode and $\Omega_i = ZeB_{0z}/m_i c$ is the cyclotron frequency of the ion with charge Z and mass $m_i = \mu m_p$, with m_p being the proton mass and *c* is the speed of light) in a weakly inhomogeneous plasma with external magnetic field $B_{0z}(x)$. As is customary in the interchange turbulence, oscillations are taken to be uniform in the direction of the magnetic field, i.e., the wave vector along the magnetic field $k_{\|} = 0$. We consider a weakly inhomogeneous high-beta plasma of slab geometry with density $n_0(x)$ in the presence of an inhomogeneous magnetic field $B_{0z}(x)$, where x is the direction of inhomogeneity. We will also retain the gravity term $\mathbf{g} = g\mathbf{e}_x$, which drives the instability of the flute modes. One of the main difference if to compare with the case of a low-beta plasma is that in a high-beta plasma the electric field in the flute oscillations is not irrotational (i.e. $\vec{\nabla} \times \mathbf{E} \neq 0$) as in the low-beta case and is written as $\mathbf{E} = -\vec{\nabla} \times \Phi - (1/c)(\partial \mathbf{A}/\partial t)$. The plasma density N can be expressed as the sum of a slowly varying component with x, the equilibrium plasma density $n_0(x)$, and a perturbed component due to interchange oscillations $\delta n(x, y, t)$. Likewise, the magnetic field is written as $B_z = B_{0z} + \delta B_z(x, y, t)$. We also assume the quasi-neutrality condition $N_e = ZN_i$. The equilibrium condition for the case under consideration can be written as

$$\kappa_B = \frac{\beta}{2}\kappa_n + \frac{g\beta_i}{2V_{Ti}^2} \tag{5.1}$$

where

$$\kappa_N = -\frac{1}{n_0}\frac{dn_0}{dx} > 0, \quad \kappa_B = \frac{1}{B_{0z}}\frac{dB_{0z}}{dx} > 0, \quad \beta_i = \frac{8\pi n_{0i} T_i}{B_0^2}$$

Parameter β_i - ion plasma beta, defines the ratio of the kinetic energy containing in plasma ions to the magnetic field energy. Below we will also use parameter $\beta_e = \frac{8\pi n_e T_e}{B_{0z}^2}$ - electron plasma beta and total plasma beta $\beta = \beta_i + \beta_e$.

To obtain the coupled nonlinear system of equations for density N, electrostatic potential Φ, and magnetic field B_z, we start from the quasi-neutrality condition

$$div\mathbf{j} = 0 \tag{5.2}$$

The continuity equation for the electron density

$$\frac{\partial N_e}{\partial t} + div(\mathrm{N}_e \mathbf{v}_e) = 0 \tag{5.3}$$

And the equation for the magnetic field in the flute-type oscillations

$$\frac{\partial \delta B_z}{\partial t} = \frac{4\pi}{c} j_x \tag{5.4}$$

To the system (5.2) - (5.4) we should add equations of motion for ions and electrons. The equations of motion for the ions are written in the form

$$m_i N_i [\frac{\partial \mathbf{v}_i}{\partial t} + (\mathbf{v}_i \cdot \vec{\nabla})\mathbf{v}_i] = q_i N_i (\mathbf{E} + \frac{1}{c}[\mathbf{v}_i \times (\mathbf{B}_0 + \delta \mathbf{B})]) - \vec{\nabla} P_i - \vec{\nabla} \vec{\pi} + m_i N_i \mathbf{g} \tag{5.5}$$

where $q_i = Ze$, and $P_i = N_i T_i$. It is also assumed that the viscosity tensor $\vec{\pi}$ contains only gyroviscosity components

$$\pi_{xx} = -\pi_{yy} = -\frac{N_i T_i}{2\Omega_i}(\frac{\partial \mathrm{v}_x}{\partial y} + \frac{\partial \mathrm{v}_y}{\partial x}) \tag{5.6}$$

$$\pi_{xy} = \pi_{yx} = \frac{N_i T_i}{2\Omega_i}(\frac{\partial \mathrm{v}_x}{\partial x} - \frac{\partial \mathrm{v}_y}{\partial y}) \tag{5.7}$$

Below it is assumed that the electric drift, the diamagnetic drift, and the gravitational drift are all of the same order, and of first order in the small parameter ε defined by:

$$\frac{\omega}{\omega_{ci}} \sim \frac{Ze\Phi}{T_i} \sim \frac{\delta B_z}{B_{0z}} \sim \frac{\delta n_i}{n_{0i}} \sim \frac{\kappa_n}{k} \sim \frac{\kappa_B}{k} \sim (k\rho_i)^2 \sim \varepsilon \tag{5.8}$$

From the ion equation of motion one can obtain an iterative solution for the ion velocity:

$$\mathbf{V}_i^{(n+1)} = -\frac{c}{B_{0z}}\mathbf{z}\times\mathbf{E} + \frac{V_{Ti}^2}{\omega_{ci}}\mathbf{z}\times\frac{\nabla n_i}{n_i} - \mathbf{z}\times\frac{\mathbf{g}}{\omega_{ci}} + \frac{1}{\omega_{ci}}\left[\mathbf{z}\times\frac{\partial \mathbf{V}_i^{(n)}}{\partial t} + \mathbf{z}\times\left(\mathbf{V}_i^{(n)}\cdot\nabla\right)\mathbf{V}_i^{(n)}\right] + \mathbf{z}\times\frac{\nabla\cdot\Pi_i^{(n)}}{m_i n_i \omega_{ci}} \tag{5.9}$$

Next, we can estimate the order of various terms:

$$\mathbf{V}_E = \frac{c}{B}\mathbf{z}\times\nabla\Phi + \frac{1}{B}\mathbf{z}\times\frac{\partial \mathbf{A}}{\partial t} \sim \frac{c}{B}k\Phi + \frac{\omega \mathbf{A}}{B} \sim V_{Ti}(k\rho_i)\left(\frac{Ze\Phi}{T_i}\right) + \frac{V_{Ti}}{k\rho_i}\left(\frac{\delta B}{B}\right)\left(\frac{\omega}{\omega_{ci}}\right) \sim V_{Ti}(k\rho_i)\varepsilon \tag{5.10}$$

$$\mathbf{V}_{Di} = \frac{T_i}{m_i \omega_{ci}}\mathbf{z}\times\nabla \ln n_i \sim V_{Ti}(k\rho_i)\left(\frac{\kappa_n}{k} + \frac{\delta n_i}{n_{0i}}\right) \sim V_{Ti}(k\rho_i)\varepsilon \tag{5.11}$$

$$\mathbf{V}_g = -\mathbf{z}\times\frac{\mathbf{g}}{\omega_{ci}} \sim \frac{g}{\omega_{ci}} \sim V_{Ti}(\rho_i k)\frac{\kappa_n}{k} \sim V_{Ti}(\rho_i k)\varepsilon \tag{5.12}$$

The zero order velocity is the equilibrium diamagnetic drift plus the gravitational drift (assuming no equilibrium electric field, $\mathbf{E}_0$):

$$\mathbf{V}_i^{(0)} = \frac{V_{Ti}^2}{\omega_{ci}}\mathbf{z}\times\frac{\nabla n_{i0}}{n_{i0}} - \mathbf{z}\times\frac{\mathbf{g}}{\omega_{ci}} = \mathbf{V}_{Di0} + \mathbf{V}_g. \tag{5.13}$$

The first iteration gives:

$$\begin{aligned}\mathbf{V}_i^{(1)} &= -\frac{c}{B_0}\mathbf{z}\times\delta\mathbf{E} + \frac{V_{Ti}^2}{\omega_{ci}}\mathbf{z}\times\frac{\nabla n_i}{n_i} + \mathbf{z}\times\frac{\nabla\cdot\boldsymbol{\Pi}^{(0)}}{m_i n_i \omega_{ci}} - \mathbf{z}\times\frac{\mathbf{g}}{\omega_{ci}} = \\ &= \mathbf{V}_E + \mathbf{V}_{Di} + \mathbf{V}_g + \mathbf{V}_{\Pi 0},\end{aligned} \tag{5.14}$$

where $\nabla\cdot\boldsymbol{\Pi}^{(0)}$ is computed at $\mathbf{V}_i^{(0)}$. And from the next iteration one obtains the following solution:

$$\mathbf{V}_i^{(2)} = -\frac{c}{B_0}\mathbf{z}\times\delta\mathbf{E} + \frac{V_{Ti}^2}{\omega_{ci}}\mathbf{z}\times\frac{\nabla n_i}{n_i} - \mathbf{z}\times\frac{\mathbf{g}}{\omega_{ci}} + \frac{1}{\omega_{ci}}\left[\mathbf{z}\times\frac{\partial\mathbf{V}_i^{(1)}}{\partial t} + \mathbf{z}\times\left(\mathbf{V}_i^{(1)}\cdot\nabla\right)\mathbf{V}_i^{(1)}\right] + \mathbf{z}\times\frac{\nabla\cdot\boldsymbol{\Pi}^{(1)}}{m_i n_i \omega_{ci}} \tag{5.15}$$

where $\nabla\cdot\boldsymbol{\Pi}^{(1)}$ is computed at $\mathbf{V}_i^{(1)}$.

5.2 Corrections to Gyroviscous Cancellation

In the case of low-beta plasma the gyroviscous flux cancels the diamagnetic flux (see for example [23] and [24]) . Below we will show that in a high-beta plasma this cancellation does not take place and as a result new terms appear in the final nonlinear equations that describe interchange turbulence. Using equation (5.5) we can write the expression for the perpendicular ion velocity keeping only the terms that are first order in ε:

$$\mathbf{V}_{\perp i} = \mathbf{V}_E + \mathbf{V}_{Di} + \mathbf{V}_g + O\left(\varepsilon^2\right) \tag{5.16}$$

For the electric drift $\mathbf{V}_E$, the diamagnetic drift $\mathbf{V}_{Di}$ and for the gravitational drift $\mathbf{V}_g$ we have the following expressions:

$$\mathbf{V}_E = -\frac{c}{B_0}\mathbf{z}\times\delta\mathbf{E}\quad,\quad \mathbf{V}_{Di} = \frac{V_{Ti}^2}{\omega_{ci}}\mathbf{z}\times\frac{\nabla n_i}{n_i}\quad,\quad \mathbf{V}_g = \frac{\mathbf{z}\times\mathbf{g}}{\omega_{ci}} \tag{5.17}$$

Now the ion continuity equation can be written as:

$$\begin{aligned}&\frac{\partial n_i}{\partial t} + \nabla\cdot\left(n_i\mathbf{V}_{\perp i}\right) + \nabla\cdot\left\{\frac{z}{\omega_{ci}}\times\left[\frac{\partial\mathbf{V}_E}{\partial t} + \left(\mathbf{V}_E\cdot\nabla\right)\mathbf{V}_{\perp i}\right]\right\} + \nabla\cdot\left(\frac{z}{\omega_{ci}}\times\frac{\partial\mathbf{V}_{Di}}{\partial t}\right) + \\ &\nabla\cdot\left\{\frac{\mathbf{e}_z}{\omega_{ci}}\times\left[\frac{\nabla\cdot\boldsymbol{\Pi}}{m_i n_i} + \left(\mathbf{V}_{Di}\cdot\nabla\right)\mathbf{V}_{\perp i}\right]\right\} = 0\end{aligned} \tag{5.18}$$

After lengthy calculations we can arrive at:

$$\vec{\nabla}\cdot\{\frac{\mathbf{e}_z}{\omega_{ci}}\times[\frac{\vec{\nabla}\cdot\vec{\vec{\pi}}}{m_i n_i}+(\mathbf{V}_{Di}\cdot\vec{\nabla})\mathbf{V}_{\perp i}]\}=\frac{n_{0i}T_i}{2\omega_{ci}B_{0z}}(\frac{\partial\Delta B_z}{\partial t}-\frac{g}{\omega_{ci}}\frac{\partial\Delta B_z}{\partial y}) \tag{5.19}$$

In a low-beta plasma relation (5.19) should be replaced by the well known gyroviscous cancellation relation (see for example [23] and [24]):

$$\vec{\nabla}\cdot\{\frac{\mathbf{e}_z}{\omega_{ci}}\times[\frac{\vec{\nabla}\cdot\vec{\vec{\pi}}}{m_i n_i}+(\mathbf{V}_{Di}\cdot\vec{\nabla})\mathbf{V}_{\perp i}]\}=0 \tag{5.20}$$

5.3 Nonlinear Equations for Description of Interchange Turbulence

Finally, with the help of relation (5.19) we can arrive at the following complicated system of nonlinear equations for density N, electrostatic potential Φ and magnetic field δB_z:

$$\frac{\partial\Delta_\perp\Phi}{\partial t}-\frac{V_{Ti}^2}{\omega_{ci}}\frac{\kappa_N+\kappa_B}{1+\frac{\beta}{2}}\frac{\partial\Delta_\perp\Phi}{\partial y}+\frac{gB_{0z}}{n_{i0}c}(1+\frac{\rho_i^2\frac{\beta_e}{2}}{1+\frac{\beta}{2}}\Delta_\perp)\frac{\partial\delta n}{\partial y}-$$

$$\frac{V_{Ti}^2}{\omega_{ci}c}(\frac{\partial\Delta_\perp\delta B_z}{\partial t}+\frac{g}{\omega_{ci}}\frac{\partial\Delta_\perp\delta B_z}{\partial y})-\frac{g}{\omega_{ci}}(\frac{\partial\Delta_\perp\Phi}{\partial y}+\frac{V_{Ti}^2}{\omega_{ci}c}\frac{B_{0z}}{n_{i0}}\frac{\partial\Delta_\perp\delta n}{\partial y})= \tag{5.21}$$

$$\frac{V_{Ti}^2}{\omega_{ci}n_{0i}}\vec{\nabla}_\perp\cdot\{\vec{\nabla}_\perp\Phi,\delta n\}+\frac{c}{B_{0z}}\{\Delta_\perp\Phi,\Phi\}$$

$$\frac{\partial\delta n}{\partial t}+\frac{c}{B_{0z}}\frac{\kappa_N+\kappa_B}{1+\frac{\beta}{2}}\frac{\partial\Phi}{\partial y}-\frac{\beta_e}{\beta_i}\frac{V_{Ti}^2}{\omega_{ci}}\frac{\kappa_B-\frac{\beta}{2}\kappa_N}{1+\frac{\beta}{2}}\frac{\partial\delta n}{\partial y}=\frac{c}{B_{0z}}\{\delta n,\Phi\} \tag{5.22}$$

$$\delta B_z=\frac{\beta}{2}\delta n \tag{5.23}$$

In equations (5.21) – (5.23) we used quasi-neutrality condition $\delta n_i=\delta n_e=\delta n$ and Poisson brackets are defined as:

$$\{a,b\}=\frac{\partial a}{\partial x}\frac{\partial b}{\partial y}-\frac{\partial a}{\partial y}\frac{\partial b}{\partial x}$$

Equations (5.21) – (5.23) describe the excitation and nonlinear evolution if compressible electromagnetic interchange modes in a finite beta plasma with inhomogeneous density and

magnetic field. As one can see, the nonlinear terms in equations (5.21) – (5.22) are rather complicated. They contain so-called vector nonlinearities (represented through Poisson brackets) which are the source for generation of large scale vortex structures coexisting with short scale spectral components produced on the nonlinear stage of modulation instability of interchange modes. Equations (5.21) – (5.23) will be used to analyze interchange turbulence and scattering of high frequency electromagnetic waves on density irregularities associated with interchange turbulence.

5.5 Instability of Interchange Modes

The dispersion equation for interchange mode instability can be obtained from the linearized system of equations (5.21) – (5.23). The dispersion relation was solved numerically for the following set of plasma parameters, roughly approximating the plasma conditions that exist in the so-called spread-F layer in the ionosphere:

$n_0 \sim 2\times10^5$ cm^{-3} - plasma density
$B_0 \sim 0.4\ G$ - magnetic field
$g \sim 500\ cm/s^2$ - gravitational constant
$T_i = T_e \sim 1.4\ eV$ - ion and electron temperature
$m_i = 16\times m_p$ - ion mass and $m_p -$ proton mass

Results of the numerical solution of the linearized dispersion equation are presented in Fig. 5.1 below. In the limit of very small β , the linear dispersion relation can be solved and the linear growth rate should scale as:

$$\gamma_{\max} = \sqrt{\kappa_N g} \tag{5.24}$$

In Fig. 5.1 we compare the growth of the energy in the density and potential fluctuations from the numerical solution of equations (5.21 –5.23) with the maximum growth rate calculated from Eq. (5.24). From Eq. (5.24), we find that $\gamma_{\max} \sim 0.0408\ s^{-1}$, or $\gamma_{\max}/\omega_{ci} \sim 1.7\times10^{-4}$. As shown in Fig. 5.1, we find that $\gamma_{\max}/\omega_{ci} \sim 1.6\times10^{-4}$ provides a reasonable fit to the code results.

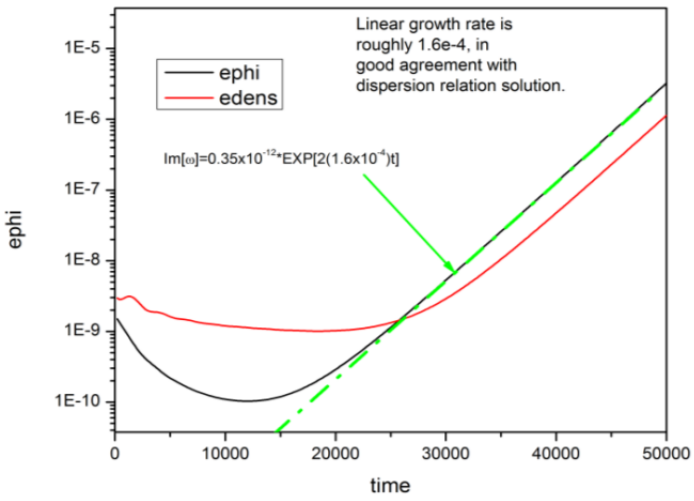

Figure 5.1. Density and potential growth

5.6 Numerical Solution of Nonlinear Equations

Below we present results of numerical solution of nonlinear system of equations (5.21) – (5.23). For the numerical analysis we use the code Flute developed by Dr. J.N. Leboeuf; detailed description of the code can be found in [17].

The linear growth of the electrostatic wave energy and density perturbations followed by the nonlinear saturation of the instability is presented in Fig. 5.2.

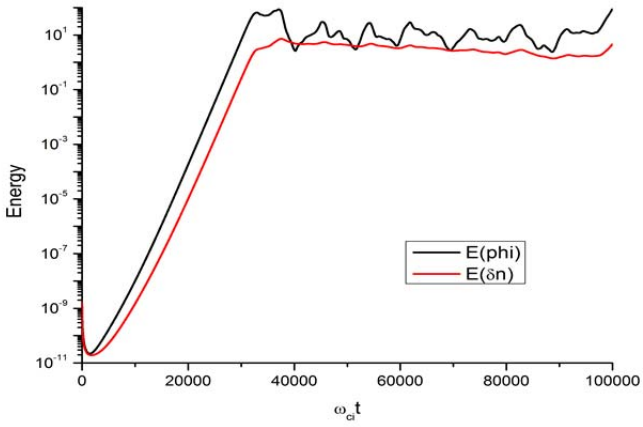

Figure 5.2. Linear growth and nonlinear saturation of the interchange instability

Snapshots of the density fluctuations are shown Fig. 5.3. The initial perturbations applied to the vorticity and density are random, with the normalized amplitude 10-4. This is illustrated in Fig. 5.3(a). The linear phase of the instability is illustrated in Fig. 5.3(b) and 5.3(c). It is clearly see that perturbations are elongated along the x – direction. This are so-called streamer-like perturbations. The transition from linear to nonlinear and the nonlinear phase is captured in Fig. 5.3(d) – (f). On the nonlinear stage, when amplitudes of perturbations exceed the threshold for the modulation instability, transition from streamer-type perturbations to the zonal flow type of perturbations (elongated along the y – direction, perpendicular to the direction of plasma inhomogeneity) takes place. This is one of the expected characteristics of the interchange turbulence. The nonlinear phase is also characterized by a broad spectrum of excited wavelengths and frequencies.

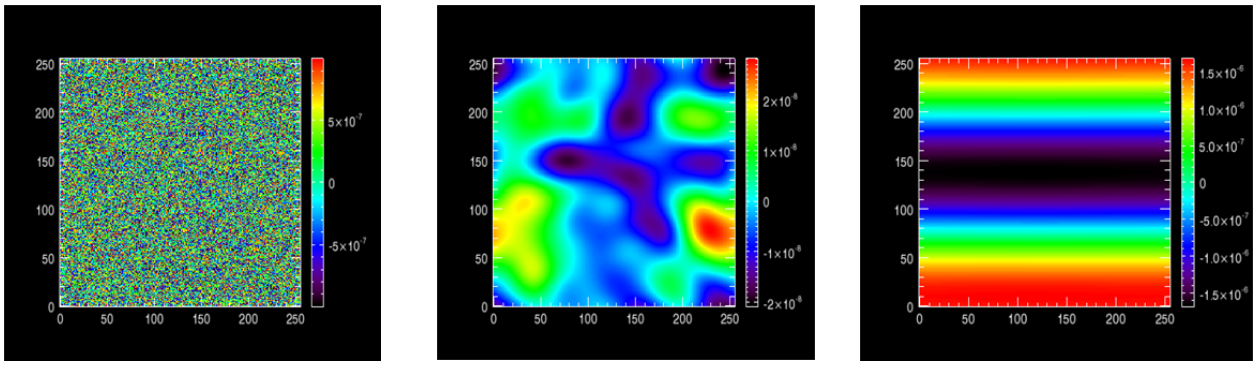

$(a)\ \ \Omega_i t = 0$ $(b)\ \ \Omega_i t = 10$ $(c)\ \ \Omega_i t = 300$

Density in linear stage

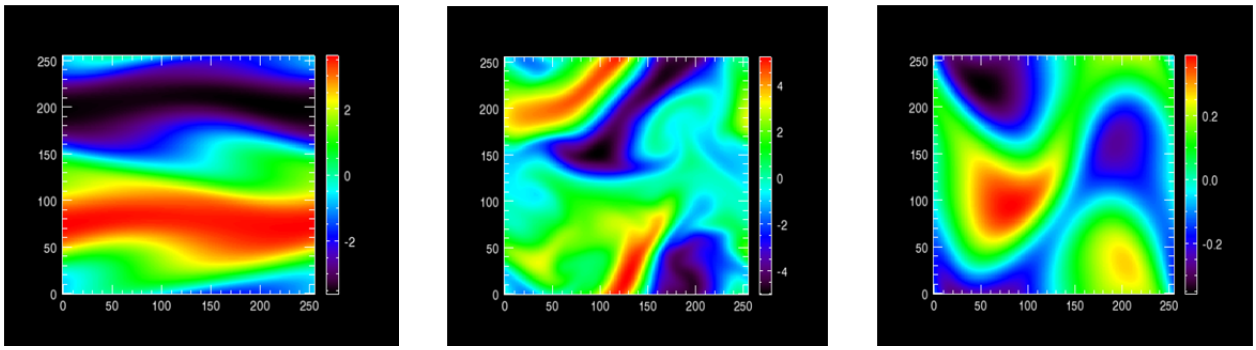

(d) $\Omega_i t = 2700$ (e) $\Omega_i t = 2800$ (f) $\Omega_i t = 2980$

Density in nonlinear stage and formation of zonal flows and nonlinear vortex structures

Figure 5.3. Snapshots of the density fluctuations

6. Summary

This paper consists of two parts. In the first part (Sections 2 – 4) results of the theoretical analysis and the NRL Space Chamber experimental study of excitation and nonlinear saturation of lower hybrid instability in plasmas with unmagnetized ions and magnetized electrons drifting across the magnetic field due to the presence of an external inhomogeneous
electric field $E_{0x}(x)$ are presented. Drifting electron flow has velocity shear and is the source of the instability (see [8,9] for details). Equation for excitation of instability in the vicinity of the lower hybrid frequency with inclusion of the thermal dispersion and electron-neutral collisions was derived and solved in nonlocal and local approximations. Results show satisfactory agreement for both numerical solution obtained with the help of the shooting code and solution in the local approximation. Next, nonlinear equations describing coupling of excited lower hybrid waves with low frequency ion acoustic perturbations were. Using these equations, modified decay instability of the lower hybrid waves in a local approximation was analyzed. In particular, dispersion equation for the modified decay instability was derived and its threshold was determined.
In the second part, analysis of interchange instability with inclusion of finite ion Larmor radius effects in a high beta plasma is presented. Obtained results are used to analyze linear and nonlinear stages of the instability as well as formation of vortex structures in a plasma with parameters similar to that in the ionospheric F layer. Numerical results show that formation of vortex structures occurs when the amplitude of density perturbations exceeds the threshold for the modulation instability and on the nonlinear stage density perturbations in the vortex structures can be very large. Developed technique can be also applied to analyze interchange modes in high energy density physics, such as Z-pinch plasmas. This study is also relevant to a laser probing in a high energy density plasmas and for diagnostics of the edge plasma in tokamaks. Another areas of applications – magnetospheric and space plasmas.
The types of density irregularities examined in the paper play important role in refraction and scattering of high frequency electromagnetic signals propagating in the earth ionosphere, inside a plasma sheath of reentry and hypersonic vehicles and in many other applications related to surveillance and navigation. Detailed analysis of high frequency electromagnetic wave refraction and scattering in the presence of developed low frequency plasma turbulence described in the paper is the subject for the future work.

Acknowledgement

This work was supported by the Air Force Research laboratory and Air Force Office of Scientific Research.

7. References

[1] J. Sheffield et al., “Plasma Scattering of Electromagnetic Radiation, Theory and Measurement Techniques”, Academic Press; 2nd edition, 2010.

[2] V.N. Tsytovich, “Theory of Turbulent Plasma”, Studies Sov. Sci., Physical Sciences, 1977.

[3] Mendonca, “Scattering of waves by Langmuir soliton”, Journal of Plasma Physics, vol. 30, 1983.

[4] Bingham et al., “Electromagnetic wave scattering in plasma”, Phys. Fluids, No. 3, p. 811, 1991.

[5] P. W. Schuck, J. W. Bonnell, and P. M. Kintner, Jr., A Review of Lower Hybrid Solitary Structures, IEEE TRANS.PLASMA SCI., 31, 1125, 2003

[6] Ganguli et al. JGR Vol. 99, p. 8873, 1994

[7] E. V. Mishin, P. A. Puhl-Quinn, and O. Santolik (2010), SAID: A turbulent plasmaspheric boundary layer, Geophys. Res. Lett., 37, L07106, doi:10.1029/2010GL042929.

[8] E. V. Mishin, and W. J. Burke (2005), Stormtime coupling of the ring current, plasmasphere, and topside ionosphere: Electromagnetic and plasma disturbances, J. Geophys. Res., 110, A07209, doi:10.1029/2005JA011021

[9] G. Ganguli, Y.C. Lee, P.J. Palmadesso, “Electron-ion hybrid mode due to transverse velocity shear”, Phys. Fluids, No. 31, p. 2753, 1988.

[10] "Electron-ion hybrid instabilities driven by velocity shera in a magnetized plasma", Phys. Fluids B, Vol 4, p 1708, 1992.

[11] W. H. Press, B. P. Flannery, S. A. Teukolsky, and W. T. Vetterling, Numerical Recipes (Cambridge University Press, Cambridge, 1989), Ch. 16.

[12] W. E. Amatucci, G. Ganguli, D.N. Walker, G. Gatling, M. Balkey, and T. McGulloch, “Laboratory investigation of boundary layer processes due to strong spatial inhomogeneity”, Phys. Plasmas, Vol. 10, No. 5, p. 1963, 2003.

[13] V.I. Sotnikov, V.D. Shapiro, V.I. Shevchenko, “Macrascopic consequences of collapse at the lower hybrid resonance”, Sov. J. Plasma Phys, Vol. 4, p. 252, 1978.

[14] V.D. Shapiro, G.I. Soloviev, J.M. Dawson, R. Bingham, “Lower hybrid dissipative cavitons and ion heating in the auroral ionosphere”, Phys. Plasmas, Vol . 2, No. 2, p. 516, 1995.

[15] R.Z. Sagdeev, V.I. Sotnikov, V.D. Shapiro, V.I. Shevchenko, “Contribution to the theory of magnetosonic turbulence”, JETP Lett., Vol. 26, No. 11, P. 582, 1977.

[16] Z. N. Andrushchenko and V. P. Pavlenko, “Turbulent generation of large scale flows and nonlinear dynamics of flute modes,” *Phys. Plasmas*, vol. 9, no. 11, pp. 4512–4519, Nov. 2002.

[17] V. I. Sotnikov, V. V. Ivanov, R. Presura, J. N. Leboeuf, O. G. Onishchenko, B. V. Oliver, B. Jones, T. A. Mehlhorn and C. Deeney, “Investigation of compressible electromagnetic flute mode instability in finite beta plasma in support of Z-pinch and laboratory astrophysics

experiments," Commun. Comput. Phys., 4 (2008), pp. 611-623.

[18] Sotnikov, V. I., V.V. Ivanov, R. Presura , E. Yassin, J. Kindel, J.N. Leboeuf, O.G. Onishchenko , B.V. Oliver , B. Jones, T.A. Mehlhorn , C. Deeney , "Investigation of flute instability in application to laboratory astrophysics and Z-pinch experiments,"Astrophys. Space Sci. (2009) 322: 209–213.

[19] M. C. Kelley, The Earth's Ionosphere: Plasma Physics and Electrodynamics, 2nd Edition, Academic Press, Amsterdam, 2009.

[20] D. L. Hysell and E. B. Shume, "Electrostatic plasma turbulence in the topside equatorial F region ionosphere," J. Geophys. Res. 107 (A10) , 1269, 2002.

[21] Hysell, D. L., M. Yamamoto, and S. Fukao, Imaging radar observations and theory of type I and type II quasi-periodic echoes, J. Geophys. Res., 107 (A11), 1360, doi:10.1029/2002JA009292 (2002).

[22] Kelley, M. C., J. J. Makela, O. de La Beaujardière, and J. Retterer, Convective ionospheric storms: A review, Rev. Geophys., 49, RG2003, doi:10.1029/2010RG000340, (2011).

[23] A.B. Mikhailovskii, "Theory of plasma instabilities", Studies of Sov. Sci., 1995.

[24] R.D. Hazeltine and J.D. Meiss, "Shear-Alfven Dynamics of Toroidally Confined Plasmas", Physics Reports, 121, pp. 1 -164, 1985.